A Contribution to the Numerical Prediction of Unsteady Flows

Maurizio Pandolfi*
Politecnico di Torino, Torino, Italy

Methods based on "flux-difference splitting" are investigated with reference to the prediction of unsteady compressible flows. They combine the feature of taking into account the wake-like nature of these flows and the capability of correctly capturing shock waves. Two recently proposed approaches and a third one suggested here are compared for one-dimensional flow, with particular reference to the means of operating the splitting. They are extended to the cases of variable-area ducts and a general transformation of the independent variables. First- and second-order accurate schemes are presented and procedures for the computation at the boundaries are shown. Finally, numerical experiments are reported and discussed.

Introduction

THE prediction of unsteady flows, described by the Euler equations, can be obtained through finite difference numerical methods. Here the time derivatives of the flow properties are evaluated on the basis of derivatives in space at a given time. The wave-like nature of these flows suggests that, in the numerical procedure of approximating the derivatives in space with finite differences, the domains of dependence have to be taken into account correctly, according to the propagation of waves through the flow. Three methods have been proposed in the literature in order to accomplish this goal: λ formulation, flux-vector splitting, and flux-difference splitting. It should be mentioned that these three methods lead to identical conclusions, conceptually and numerically, for the particular case of a system of linear hyperbolic equations.

The λ formulation was proposed several years ago[1] and has been applied to a variety of multidimensional flows since then. A proper formulation of the original Euler equations puts in evidence the role of the Riemann invariants, or similar parameters, and the respect of the domains of dependence is achieved by looking at the direction of the propagation of small disturbances. The codes are simple, the computing time is kept very low (an essential feature for multidimensional flows), and the accuracy of the results is very satisfactory. However, in most of the cases, shock waves have to be treated explicitly, in a more or less complicated manner, in order to correctly evaluate their propagation.

In the "flux-vector splitting" and "flux-difference splitting" methods the Euler equations are written in a divergence form and the shock waves are captured numerically.

The recently proposed[2] "flux-vector splitting" also aims to respect the domains of dependence. It may be recognized that the flux vector f can be divided in three terms related to the corresponding characteristics. At each computational point the vector f is then split into two subvectors (f^+, f^-), each including those terms associated with the characteristics propagating with positive (f^+) or negative (f^-) velocity. The algorithm is based on upwind schemes, where the one-sided differences are evaluated up- or downstream for each of the two subvectors.

The "flux-difference splitting" method can be considered a development of the original ideas reported in Ref. 3. Here the attention is focused on the difference in the flux between two neighboring computational points. Such a difference is split into terms that will affect the flow evolution at points located on the left or right of the interval. The criteria for splitting the flux difference can be different. For instance, Ref. 4 presents an interesting way of performing the splitting. However, we are more interested in other recent methods[5,6] that can be integrated on the basis of a discretized model of the flow. The properties of the stream at each computational point are assumed to represent uniform flow over the cell extending for one-half grid interval on the two sides of the nodal point. A discontinuity will generally separate two neighboring cells in the middle of the interval. The evolution in time of this discontinuity (the solution of a Riemann problem) provides the nature of the three waves generated here and the criteria for splitting the difference of the flux over an interval into terms associated with waves that may move up- or downstream. Also, here the algorithm is based on upwind schemes in connection with the terms in which the flux difference has been split.

The present paper aims to contribute to the development of the "flux-difference splitting" method. An approach somewhere between the two proposed in Refs. 5 and 6 is presented and compared with them. An extension is shown to the cases of variable cross-section ducts and of a general transformation of the primitive independent variables. First- and second-order accurate schemes are considered and procedures for the computation at the boundaries are presented. Several numerical examples are shown and discussed.

Flow in Constant-Area Ducts

The Euler equations are written in a divergence form

$$w_t + f_x = 0 \tag{1}$$

where

$$w = \begin{vmatrix} \rho \\ \rho u \\ e \end{vmatrix} \qquad f = \begin{vmatrix} \rho u \\ p + \rho u^2 \\ u(p+e) \end{vmatrix}$$

The nomenclature is the usual one: density ρ, pressure p, gas velocity u, speed of sound a, total energy per unit volume e, space x, and time t.

Let us consider the discretized representation of the flow, where the values of the variables (ρ_i, u_i, e_i) at the time t_0 are given at the computational points located at $x_i = (i-1)\Delta x$. Let us also define the difference $\Delta_i f = f_{i+1} - f_i$. The corresponding term $(\Delta_i f \cdot \Delta t / \Delta x)$ may be interpreted as the contribution of

Presented as Paper 83-0121 at the AIAA 21st Aerospace Sciences Meeting, Reno, Nev., Jan. 10-13, 1983; submitted Feb. 5, 1983; revision received June 24, 1983.

*Professor, Istituto di Macchine e Motori per Aeromobili.

the interval $(x_{i+1}-x_i)$ to the variation in time from t_0 to $t_0+\Delta t$ of the vector w. The wave-like nature of these flows indicates which points will be affected by the difference $\Delta_i f$. In particular cases, the difference $\Delta_i f$ influences points located on only one side of the interval, as in regions of supersonic flow when the three characteristics propagate in the same direction or in "simple wave" flows where, even with characteristics propagating in opposite directions, the difference $\Delta_i f$ contributes wholly to one wave. However, in general, the speeds of propagation of the waves show different signs and the signals carried on them are not zero. Therefore, it seems convenient to split the difference $\Delta_i f$ in distinct terms that will affect, respectively, points up- or downstream of the considered interval.

In order to accomplish this goal, let us model the flow at time t_0 over the interval $(x_{i+1}-x_i)$ with uniform flow (w_i) in the first half-interval $(x_{i+\frac{1}{2}}-x_i)$ and uniform flow (w_{i+1}) in the second half-interval $(x_{i+1}-x_{i+\frac{1}{2}})$. A discontinuity $(\Delta_i w$ and/or $\Delta_i f)$ is then separating the two half-intervals and is located at the middle $(x_{i+\frac{1}{2}})$. It is now required to predict the evolution in time of this discontinuity (solution of a Riemann problem). With reference to Fig. 1, the interaction between the two regions (a$=i$ and b$=i+1$) will generate two further uniform regions (c and d) separated by waves 1-3, which correspond to the families of characteristics ($u-a$, u, and $u+a$). Wave 2 describes a contact surface, while waves 1 and 3 can represent shock waves or expansion fans. In the case of Fig. 1, where waves 2 and 3 travel rightward, the signals carried over them (the difference of the flux between regions b and d over wave 3 and that between regions d and c over wave 2) bring the proper information for the evolution in time of w to points located at the right side of the interval, while the signal on wave 1 (the difference between regions c and a) affects points on the left side. The difference of the flux through the initial discontinuity $\Delta_i f$ is then split into three terms,

$$\Delta_i f=(\Delta_i f)_1+(\Delta_i f)_2+(\Delta_i f)_3$$
$$=(f_c-f_a)+(f_d-f_c)+(f_b-f_d) \tag{2}$$

which contribute to the evolution in time of w in points about the interval according to the direction of propagation of the corresponding waves (1-3).

The exact solution of this Riemann problem (Fig. 1) involves a computational effort with iterative procedures because of possible shocks, which may not be negligible. On the other hand, as reported in Ref. 5 and as proved by numerical experiments, such an exact solution is not essential to get good numerical results. On the contrary, it is convenient to solve the Riemann problem approximately, thus saving computing time and gaining coding simplicity without severe penalties on the quality of the final numerical results. In particular, the two approaches suggested in Refs. 5 and 6 and the one proposed here differ on the procedure to obtain the approximate solution. In the following, they will be referred to as APP1, APP2, and APP3, respectively.

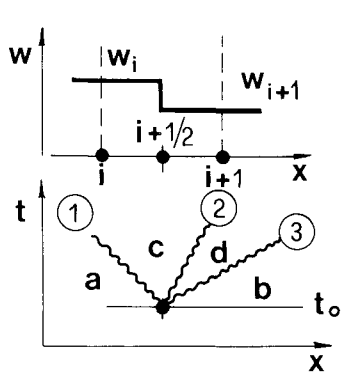

Fig. 1 Riemann problem. Evoluton of the discontinuity located in the middle of a grid.

Approach APP1

The procedure followed by this approach is given in Ref. 5 and in more detail in Ref. 7. A short description is reported here.

A suitable matrix $\tilde{A}$ is constructed, which in addition to satisfying a list of definite properties, relates the difference $\Delta_i f$ and $\Delta_i w$ as

$$\Delta_i f=\tilde{A}\Delta_i w \tag{3}$$

The elements of $\tilde{A}$ depend on the flow properties at points i and $i+1$ and are written in terms of the following parameters:

$$\tilde{u}=\frac{\rho_i^{1/2}u_i+\rho_{i+1}^{1/2}u_{i+1}}{\rho_i^{1/2}+\rho_{i+1}^{1/2}} \qquad \tilde{H}=\frac{\rho_i^{1/2}H_i+\rho_i^{1/2}H_{i+1}}{\rho_i^{1/2}+\rho_{i+1}^{1/2}}$$
$$a=\sqrt{(\gamma-1)(\tilde{H}-u^2/2)} \tag{4}$$

The eigenvalues of $\tilde{A}$ are given by

$$\tilde{\lambda}_1=\tilde{u}-\tilde{a}, \qquad \tilde{\lambda}_2=\tilde{u}, \qquad \tilde{\lambda}_3=\tilde{u}+\tilde{a}$$

and the corresponding eigenvectors are

$$r_1=\begin{vmatrix}1\\ \tilde{u}-\tilde{a}\\ \tilde{H}-\tilde{u}\tilde{a}\end{vmatrix} \qquad r_2=\begin{vmatrix}1\\ \tilde{u}\\ \tilde{u}^2/2\end{vmatrix} \qquad r_3=\begin{vmatrix}1\\ \tilde{u}+\tilde{a}\\ \tilde{H}+\tilde{u}\tilde{a}\end{vmatrix} \tag{5}$$

The difference $\Delta_i w$ is then projected onto these eigenvectors

$$\Delta_i w=\alpha_1 r_1+\alpha_2 r_2+\alpha_3 r_3 \tag{6}$$

Once the values of w_i, w_{i+1} are prescribed, it is possible to obtain the components α_1, α_2, and α_3. Furthermore, owing to Eq. (3), one has

$$\Delta_i f=\tilde{\lambda}_1\alpha_1 r_1+\tilde{\lambda}_2\alpha_2 r_2+\tilde{\lambda}_3\alpha_3 r_3 \tag{7}$$

Here, the difference $\Delta_i f$ appears split into three terms, each associated with a corresponding eigenvalue. In other words, the nonlinear problem of Fig. 1 is approximated by an "equivalent" linear problem.

It is easy to recognize the meaning of the terms in the right sides of Eqs. (6) and (7). Starting from the initial regions (a,b), two new uniform regions ($\tilde{c}$,$\tilde{d}$) are generated. All of these regions are separated by three lines ($\tilde{1}$,$\tilde{2}$,$\tilde{3}$) defined by the eigenvalues ($\tilde{\lambda}_1$,$\tilde{\lambda}_2$,$\tilde{\lambda}_3$) that approximate waves 1-3 of Fig. 1. Whereas waves 1 and 3 can be either shock waves (discontinuity lines) or expansion fans (finite regions of smooth transition between regions a,c or b,d), the passages from region a to $\tilde{c}$ and region b to $\tilde{d}$ are discontinuous and the possible expansion fans are approximated by lines of discontinuity. The three terms into which $\Delta_i w$ is split in Eq. (6),

$$(\tilde{\Delta}_i w)_1=\alpha_1 r_1 \qquad (\tilde{\Delta}_i w)_2=\alpha_2 r_2 \qquad (\tilde{\Delta}_i w)_3=\alpha_3 r_3$$

can be regarded as the jumps of w from region $\tilde{c}$ to a (through $\tilde{1}$), from region $\tilde{c}$ to $\tilde{d}$ (through $\tilde{2}$), and from region $\tilde{d}$ to b (through $\tilde{3}$), respectively. Furthermore, the three terms in Eq. (7)

$$(\tilde{\Delta}_i f)_1=\tilde{\lambda}_1\alpha_1 r_1 \qquad (\tilde{\Delta}_i f)_2=\tilde{\lambda}_2\alpha_2 r_2 \qquad (\tilde{\Delta}_i f)_3=\tilde{\lambda}_3\alpha_3 r_3$$

can be interpreted as the corresponding jumps of f. These three terms approximate the splitting seen in Eq. (2).

Approach APP2

The exhaustive description of this approach is given in Ref. 6. Here it is interpreted with reference to the model of Fig. 1 in a form suitable for the comparison with the other two approaches. A basic hypothesis is made in APP2 (as well as in APP3) by assuming the evolution through waves 1 and 3 to be isentropic even if they actually can represent shock waves. The prescribed distribution of w in $(x_{i+1}-x_i)$ at time t_0 can be regarded as generated by waves 3″, 2″, and 1″, which converge in $x_{i+1/2}$ at t_0 and identify regions c″ and d″ as shown in Fig. 2. Owing to the previous assumption about the entropy, it is easy to evaluate the flow in regions c″ and d″, once those in regions a and b are prescribed,

$$\frac{2}{\gamma-1}a_{c''}-u_{c''}=\frac{2}{\gamma-1}a_a-u_a \qquad S_{c''}=S_a$$

$$\frac{2}{\gamma-1}a_{d''}+u_{d''}=\frac{2}{\gamma-1}a_b+u_b \qquad S_{d''}=S_b$$

$$u_{c''}=u_{d''} \qquad a_{c''}=a_{d''}\exp[(S_{c''}-S_{d''})/(2\gamma)] \tag{8}$$

The values of the flux in regions c″ and d″ are then known. Then, the evolution of discontinuity $\Delta_i w$ at time t_0 generates regions c′ and d′, separated from each other by wave 2′ and from regions a and b by waves 1′ and 3′, respectively. The terms $(\Delta_i f)_{1,2,3}$ of Eq. (2) are now approximated as follows:

$$(\Delta_i f)_1 \simeq (f_{c'}-f_a) \simeq (f_b-f_{d''})$$

$$(\Delta_i f)_2 \simeq (f_{d'}-f_{c'}) \simeq (f_{d''}-f_{c''})$$

$$(\Delta_i f)_3 \simeq (f_b-f_{d'}) \simeq (f_{c''}-f_a) \tag{9}$$

In the case where waves 1 and 3 are expansions, this procedure will provide a solution of the Riemann problem almost exactly, owing to the minor assumption of neglecting the differences of the flux through waves 1″, 2″, and 3″ with respect to those through 1′, 2′, and 3′. However, if at least one of wave 1 or 3 is represented by a shock, then its entropy variation is neglected and the solution of the Riemann problem becomes approximated. In fact, any possible shock is replaced by a converging fan of characteristics. In any case, waves 1″ and 3″ are simulated by fans of characteristics, converging (shock waves) or diverging (expansion fans). The slopes of the characteristics delimiting the fans are known. In the case of wave 3″, the fan is bounded by (u_a+a_a) and $(u_{c''}+a_{c''})$, while for wave 1″ it is confined by (u_b-a_b) and $(u_{d''}-a_{d''})$. A remarkable feature of this approach arises when a fan simulating a wave (3″ or 1″) contains a characteristic vertical in the plane (x, t).

Let us assume (Fig. 3a) that wave 1″ simulates a shock with a converging fan bounded by $(u_{d''}-a_{d''})>0$ and $(u_b-a_b)<0$. The flow properties over the vertical characteristic q are given by

$$\frac{2}{\gamma-1}a_q+u_q=\frac{2}{\gamma-1}a_b+u_b \qquad u_q=a_q \qquad S_q=S_b \tag{10}$$

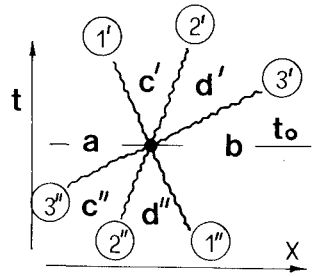

Fig. 2 Solution of the Riemann problem in approaches APP1, APP2, and APP3.

and the flux f_q is easily computed. The flux difference is then split as

$$\Delta_i f=(f_b-f_q)+(f_q-f_{d''})+(f_{d''}-f_{c''})+(f_{c''}-f_a) \tag{11}$$

Now the terms $(\Delta_i f)_2=(f_{d''}-f_{c''})$ and $(\Delta_i f)_3=(f_{c''}-f_a)$ associated with waves 2″ and 3″ contribute to the evolution in time of w at points on the right of the interval, while the contribution of wave 1″, $(\Delta_i f)_1=(f_b-f_{d''})$, is separated in two parts: one (f_b-f_q) affects points on the left, whereas the other $(f_q-f_{d''})$ refers to points at the right of the interval. In the case, wave 1″ represents an expansion (Fig. 3b) that is a diverging fan, the sides influenced by the two parts of $(\Delta_i f)_1$ are reversed.

Approach APP3

A third approach is proposed in this paper, which follows the physical interpretation of APP1 as regards the interaction of Fig. 1, but appears very similar to APP2. As in APP2, it is assumed that no entropy variations occur through waves 1 and 3, so that a fast prediction is allowed for computing the flow properties in regions c′ and d′, which approximate regions c and d of Fig. 1. Following a procedure close to what was done in APP2, one has,

$$\frac{2}{\gamma-1}a_{c'}+u_{c'}=\frac{2}{\gamma-1}a_a+u_a \qquad S_{c'}=S_a$$

$$\frac{2}{\gamma-1}a_{d'}-u_{d'}=\frac{2}{\gamma-1}a_b-u_b \qquad S_{d'}=S_b$$

$$u_{c'}=u_{d'} \qquad a_{c'}=a_{d'}\exp[(S_{c'}-S_{d'})/(2\gamma)] \tag{12}$$

The values of the flux in regions c′ and d′ are then computed and the terms in which $\Delta_i f$ is split, according to Eq. (2), are

$$(\Delta_i f)_1=f_{c'}-f_a \qquad (\Delta_i f)_2=f_{d'}-f_{c'} \qquad (\Delta_i f)_3=f_b-f_{d'} \tag{13}$$

As in APP2, waves 1′ and 3′ are represented by converging or diverging fans. It is possible that a characteristic inside a fan is vertical.

If, as in Fig. 4a, wave 1′ simulates a shock with a converging fan bounded by $(u_{c'}-a_{c'})<0$ and $(u_a-a_a)>0$, the conditions on this characteristic (r) are given by

$$\frac{2}{\gamma-1}a_r+u_r=\frac{2}{\gamma-1}a_a+u_a \qquad u_r=a_r \qquad S_r=S_a \tag{14}$$

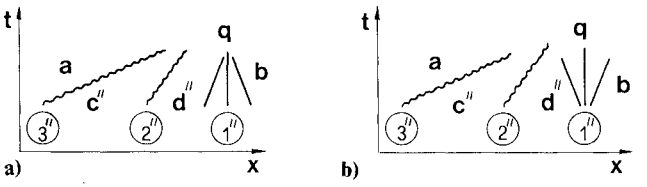

Fig. 3 Pattern of waves with a sonic point in approach APP2.

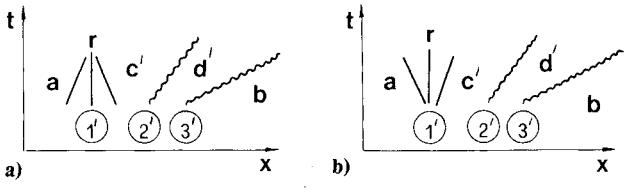

Fig. 4 Pattern of waves with a sonic point in approach APP3.

and the flux f_r is computed easily. The difference $\Delta_i f$ is now divided into

$$\Delta_i f = (f_b - f_{d'}) + (f_{d'} - f_{c'}) + (f_{c'} - f_r) + (f_r - f_a) \qquad (15)$$

The terms $(\Delta_i f)_2 = (f_{d'} - f_{c'})$ and $(\Delta_i f)_3 = (f_b - f_{d'})$ associated with waves 2′ and 3′ contribute to the evolution of w at points on the right of the interval. On the other hand, the term $(\Delta_i f)_1 = (f_{c'} - f_a)$ is divided into two parts affecting points located, respectively, on the left $(f_{c'} - f_r)$ and on the right $(f_r - f_a)$ of the interval. In this case, wave 1′ represents an expansion, that is a diverging fan (Fig. 4b), the sides affected by the two parts of $(\Delta_i f)_1$ are reversed, just as in APP2.

The APP3 approach may then be considered a variation of APP2. However, there are some differences, which can be seen in Fig. 5, where the representations of Eqs. (8) and (10) for APP2 and Eqs. (12) and (14) for APP3 are given.

Let us assume that the given values of w_i and w_{i+1} (corresponding to regions a and b) are such that the interaction corresponds to the pattern of Figs. 3b and 4b. Points A and B located on the vertical planes at $S = S_a$ and $S = S_b$ refer to the flow in regions a and b. According to APP2, the splitting is based on the path AC″D″B, with the sonic point Q. The resulting splitting gives

$$\Delta_i f = \Delta_i \overleftarrow{f} + \Delta_i \overrightarrow{f} \quad \Delta_i \overleftarrow{f} = (f_q - f_{d''})$$
$$\Delta_i \overrightarrow{f} = (f_b - f_q) + (f_{d''} - f_a) \qquad (16)$$

where $\Delta_i \overleftarrow{f}$ and $\Delta_i \overrightarrow{f}$ contribute to points located at the left and right of the interval $(x_{i+1} - x_i)$, respectively.

The splitting based upon APP3 follows the path AC′D′B with the sonic point R. The flux difference is now split as

$$\Delta_i f = \Delta_i \overleftarrow{f} + \Delta_i \overrightarrow{f} \quad \Delta_i \overleftarrow{f} = (f_r - f_a) \quad \Delta_i \overrightarrow{f} = (f_b - f_r) \qquad (17)$$

Both approaches approximate the splitting obtainable from the exact solution of the Riemann problem, as shown in Fig. 6. If we represent the exact splitting in Fig. 5, the path turns out to be ACDB, with a sonic point at R. Note that the splitting used in APP3 and the exact one coincide, even if their paths do not.

Variable-Area Duct and Transformation of the Independent Variables

The Euler equations for cross area A variable with x, can be written as

$$w_t + f_x + g = 0 \qquad (18)$$

where:

$$w = \begin{vmatrix} \rho A \\ \rho u A \\ eA \end{vmatrix} \quad f = \begin{vmatrix} \rho u A \\ (p + \rho u^2) A \\ u(p+e)A \end{vmatrix} \quad g = \begin{vmatrix} 0 \\ -pA_x \\ 0 \end{vmatrix}$$

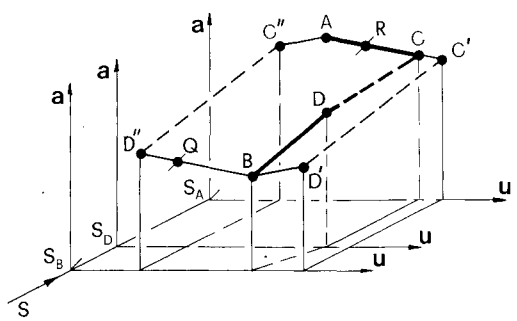

Fig. 5 Interpretation of the splittings in approaches APP2 and APP3 and for the exact solution of a Riemann problem.

In some cases it may be convenient to introduce a transformation of the independent variables, such as $X = X(x,t)$ and $T = t$, in order to use a stretching along x and to consider moving boundaries (piston problems). The equations of motion [Eq. (18)] then become

$$W_T + F_X + G = 0 \qquad (19)$$

where

$$W = \begin{vmatrix} \rho A/X_x \\ \rho u A/X_x \\ eA/X_x \end{vmatrix} \quad F = \begin{vmatrix} \rho u A + \rho A X_t/X_x \\ (p+\rho u^2)A + \rho u A X_t/X_x \\ u(p+e)A + eAX_t/X_x \end{vmatrix} \quad G = g$$

With reference to the interval $(X_{i+1} - X_i)$, the term $F_X + G$ can be approximated with

$$F_X + G \simeq (\Delta_i F^* + G^*)/\Delta X$$

where

$$\Delta_i F^* = \begin{vmatrix} \Delta_i [\rho u \bar{A} + \rho(\overline{AX_t/X_x})] \\ \Delta_i [(p+\rho u^2)\bar{A} + \rho u(\overline{AX_t/X_x})] \\ \Delta_i [u(p+e)\bar{A} + e(\overline{AX_t/X_x})] \end{vmatrix}$$

$$G^* = \begin{vmatrix} \overline{\rho u}\Delta_i A + \bar{\rho}\Delta_i(AX_t/X_x) \\ \overline{\rho u^2}\Delta_i A + \overline{\rho u}\Delta_i(AX_t/X_x) \\ \overline{u(p+e)}\Delta_i A + \bar{e}\Delta_i(AX_t/X_x) \end{vmatrix}$$

Here the bar denotes an arithmetic mean value. For example,

$$\overline{\rho u} = \tfrac{1}{2}(\rho_i u_i + \rho_{i+1} u_{i+1})$$

The term $\Delta_i F^*$ involves differences of the flow-dependent variables (w,f), whereas G^* refers to differences related to the transformation of the independent variables and to the prescribed pattern of the area. The difference $\Delta_i F^*$ now will be divided into parts in a way similar to that previously done for $\Delta_i f$ in APP1, APP2, and APP3, as reported in Ref. 9.

Integration Schemes and Computation at the Boundaries

As it has been seen, in the above three approaches, it is possible to divide the difference $\Delta_i f$ into three contributions associated to the corresponding waves. Moreover, in APP2 and APP3 the contribution of one of the waves (1 or 3) can be divided further in the case of a sonic transition.

According to the first-order upwind scheme, the flow properties w_i^{k+1} at the time $t_0 + \Delta t$ can be computed, starting from w_i^k at t_0, as it follows:

$$w_i^{k+1} = w_i^k - (\Delta t/\Delta x)(\Delta_{i-1} \overrightarrow{f} + \Delta_i \overleftarrow{f}) \qquad (20)$$

where $\Delta_{i-1} \overrightarrow{f}$ includes the contributions of the interval $(x_i - x_{i-1})$ associated with waves traveling rightward, and $\Delta_i \overleftarrow{f}$ refers to the contributions of the interval $(x_{i+1} - x_i)$

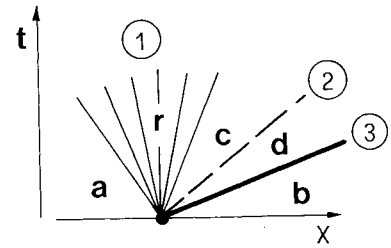

Fig. 6 Pattern of the waves, with a sonic point (r) into wave 1, obtained from the exact solution of a Riemann problem.

associated with leftward running waves. At a boundary point, the variation in time of w is determined by the interaction of the waves coming from the interval next to the boundary, with the conditions prescribed at the boundary itself. The computation here proceeds in two steps. First, the value $\underline{w}_i^{k+1}$ is computed by using the only available contributions in Eq. (20), $\Delta_{i-1}^{\rightarrow} f$ or $\Delta_i^{\leftarrow} f$ for right or left boundary. In the second step, the suggestion given in Ref. 10 is followed. The value of $\underline{w}_i^{k+1}$ is corrected in the final w_i^{k+1} by imposing the boundary conditions. In doing this, one accepts as correct those terms associated with the characteristics impinging upon the boundary from the inner flow region. The boundary condition provides the remaining information. A similar procedure has recently been proposed in Ref. 8. Three kinds of boundaries are briefly discussed here. The extension to different cases is straightforward.

In the case of inlet subsonic flow ($i=1$), the boundary conditions are given by prescribing at each instant of time the total temperature θ_{in1}° and the entropy S_{in1}. The Riemann invariant, associated with the only characteristic reaching the inlet, is accepted as correct. The following relationships lead to the final value of w_1^{k+1}.

$$\frac{2}{(\gamma-1)} a_1^{k+1} - u_1^{k+1} = \frac{2}{(\gamma-1)} \underline{a}_1^{k+1} - \underline{u}_1^{k+1}$$

$$\frac{2}{(\gamma-1)} (a_1^{k+1})^2 + (u_1^{k+1})^2 = \frac{2\gamma}{(\gamma-1)} \theta_{in1}^{\circ} \qquad S_1^{k+1} = S_{in1}$$

In the case of supersonic inlet flow, the value of w_1^{k+1} is completely determined by the prescribed corresponding set of boundary conditions.

In the case of subsonic outlet flow ($i=ic$, where $ic-1$ is the number of intervals) with a prescribed value of pressure (p_{ex}) in the downstream capacity, one Riemann invariant and the entropy, which are associated with the two characteristics ($u+a$, u) reaching the outlet, are accepted as correct. The following relationships allow for the evaluation of w_{ic}^{k+1}:

$$\frac{2}{(\gamma-1)} a_{ic}^{k+1} + u_{ic}^{k+1} = \frac{2}{(\gamma-1)} \underline{a}_{ic}^{k+1} + \underline{u}_{ic}^{k+1} \qquad S_{ic}^{k+1} = \underline{S}_{ic}^{k+1}$$

$$a_{ic}^{k+1} = \sqrt{\gamma} p_{ex}^{(\gamma-1)/(2\gamma)} \exp[\underline{S}_{ic}^{k+1}/(2\gamma)]$$

When the flow is supersonic at the outlet, the value w_{ic}^{k+1} no correction is required.

In the case where the boundary (for example, $i=1$) is a wall moving with the prescribed velocity U like a piston, one Riemann invariant and the entropy are accepted as correct and the gas velocity is imposed ($u_1^{k+1}=U$). The final value of w_1^{k+1} is computed by

$$\frac{2}{(\gamma-1)} a_1^{k+1} - u_1^{k+1} = \frac{2}{(\gamma-1)} \underline{a}_1^{k+1} - \underline{u}_1^{k+1}$$

$$S_1^{k+1} = \underline{S}_1^{k+1} \qquad u_1^{k+1} = U$$

More accurate results can be obtained by a second-order scheme. Here Fromm's scheme has been used. For the linear scalar equation

$$z_t + K z_x = 0 \qquad (K = \text{const} > 0)$$

such a scheme is written in the following form:

$$z_i^{k+1} = z_i^k - \sigma(z_i^k - z_{i-1}^k) - \sigma\left(\frac{1-\sigma}{4}\right)[(z_{i+1}^k - z_i^k) - (z_{i-1}^k - z_{i-2}^k)]$$

where $\sigma = K \cdot \Delta t/\Delta x$. It should soon be recognized that the second-order term involves a violation of the domain of dependence (for $z_{i+1}^k - z_i^k$), but the numerical results do not seem to be affected appreciably by this infringement. Spurious numerical wiggles originating near captured shocks are eliminated by following the criterium given by Eq. (67) of Ref. 11, where the above second-order term is replaced by a suitable approximation. In the case of the Euler equations [Eq. (1)], this procedure is applied to each of the terms associated with the corresponding waves into which $\Delta_i f$ has been divided. The procedure is shown in the following. Assume, for example, the patterns of interaction in the intervals about the point i, as shown in Fig. 1, where wave 1 runs leftward and waves 2 and 3 rightward. From the splitting at each interval $(x_{j+1} - x_j)$ one has

$$\Delta_j f = (\Delta_j f)_1 + (\Delta_j f)_2 + (\Delta_j f)_3$$

The three terms $(\Delta_j f)_{1,2,3}$ are approximated in Eq. (7) for APP1, in Eq. (9) for APP2, and in Eq. (13) for APP3. Let us define suitable values of the speed of waves 1-3. In APP1 they result in

$$(\lambda_j)_1 = \tilde{u} - \tilde{a} \qquad (\lambda_j)_2 = \tilde{u} \qquad (\lambda_j)_3 = \tilde{u} + \tilde{a}$$

In APP3 they will be

$$(\lambda_j)_1 = [(u_a - a_a) + (u_{c'} - a_{c'})]/2 \qquad (\lambda_j)_2 = u_{c'}$$

$$(\lambda_j)_3 = [(u_{d'} + a_{d'}) + (u_b + a_b)]/2$$

and in APP2 the same with regions c″ and d″. The first-order term in the scheme is

$$E_1 = -(\Delta t/\Delta x)[(\Delta_{i-1} f)_3 + (\Delta_{i-1} f)_2 + (\Delta_i f)_1]$$

In the second-order term, we may consider that the part to accomplish is the second-order in x,

$$E_{2x} = -\frac{1}{4}\frac{\Delta t}{\Delta x}[(\Delta_i f)_3 - (\Delta_{i-2} f)_3 + (\Delta_i f)_2 - (\Delta_{i-2} f)_2 + (\Delta_{i+1} f)_1 - (\Delta_{i-1} f)_1]$$

and the part related to the second-order in time,

$$E_{2t} = \frac{1}{4}\left(\frac{\Delta t}{\Delta x}\right)^2 [(\lambda_i)_3 (\Delta_i f)_3 - (\lambda_{i-2} f)_3 (\Delta_{i-2} f)_3 + (\lambda_i)_2 (\Delta_i f)_2 - (\lambda_{i-2})_2 (\Delta_{i-2} f)_2 + (\lambda_{i+1})_1 (\Delta_{i+1} f)_1 - (\lambda_{i-1})_1 (\Delta_{i-1} f)_1]$$

The integration scheme is then given by

$$w_i^{k+1} = w_i^k + E_1 + E_{2x} + E_{2t}$$

The computation at a boundary point and at its neighbor (for example, $i=1,2$) now has to follow a procedure different from the first-order case, because in the second-order term one needs the knowledge of the contributions relative to the interval behind the first one, which does not exist at all. However, for computing the flow at $i=2$, one may follow the suggestion proposed in Ref. 12. First, the value of $\underline{w}_1^{k+1}$ is computed with the first-order scheme. Then this value is corrected on the basis of the boundary condition and the first-order final value $(w_1^{k+1})'$ is obtained. The correction $[(w_1^{k+1})' - \underline{w}_1^{k+1}]$ can be interpreted as the suitable contribution $(\Delta_0^{\rightarrow} f)$ of a fictitious interval behind the boundary. Once $(\Delta_0^{\rightarrow} f)$ is available, it is possible to proceed with the

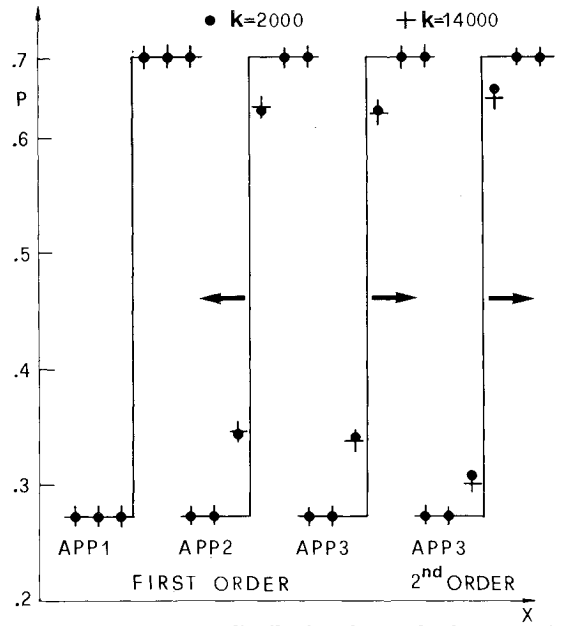

Fig. 7 Computed pressure distribution for a shock at rest in a constant-area duct.

second-order computation at $i=2$. The second-order computation at $i=1$ should require the knowledge of $\Delta_0 f$, which is not available because it does not present any physical meaning. It can be obtained by a linear extrapolation from $\Delta_1 f$ and $\Delta_2 f$. Such an estimate of $\Delta_0 f$ corresponds to replacing the approximation of the second derivative in x evaluated at $x_{1+1/2}$ with that evaluated at x_2.

Numerical Experiments

A large number of numerical experiments has been performed. In this section, some of the more significant will be discussed, starting with the simplest but not necessarily the least interesting.

Shock at Rest in a Constant-Area Duct

The initial conditions are represented by a prescribed inlet supersonic flow (M_{in1}), a shock located at the middle of the duct, and a subsonic outlet at the pressure level suitable to get the shock at rest. Physically the shock is not stable in the sense that there are no elements to define its location and any disturbance can move it extensively. Figure 7 shows the prescribed pressure distribution ($M_{in1}=1.5$) with solid lines. The computations start from this configuration and the integration in time should present numerical solutions in agreement with these initial data. The symbols in Fig. 7 denote the results obtained by APP1, APP2, and APP3 with the first-order scheme and by APP3 with the second-order scheme. With APP1, the numerical results remain unchanged with respect to the initial data, no matter how many steps of integration are done. With APP2, some steps are required for the numerical transition to a configuration that seems to remain unchanged in time. The circles denote the results at $k=2000$, with the shock transition spread over three intervals and about 70% of the jump located in the mean interval. However, as the computation goes further, the shock tends to move continuously upstream against the supersonic flow, as the results at $k=14{,}000$ (crosses) show. The speed of the captured shock results in an order of magnitude of the last significant figure of the computer. The constant-area duct is not able to stabilize the shock, whereas (as shown in the following) a slight divergence of the duct stabilizes it completely. For practical purposes, this shifting of the shock location can be neglected. The same type of results are found with APP3, except that the results shift in the opposite direction. The numerical solution obtained by APP3 with the second-order scheme is shown at the right of Fig. 7. The shock transition is sharper, with about 85% of the jump located in the mean interval, but even here the shock tends to move slightly downstream.

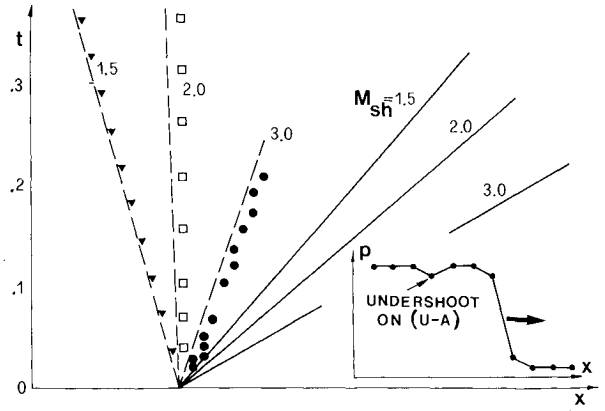

Fig. 8 Propagation of numerical perturbations generated during the formation of a captured shock.

Generation of the Transition through Shocks

During the first steps of integration, it is interesting to follow the transient from the initial prescribed step configuration of a shock to the smooth transition of the captured shock. Some results are shown in Fig. 8 and refer to the second-order scheme with APP3 for the case of a shock propagating from left to right in a gas at rest. The initial data describe the shock by a step distribution. As the integration starts, the shock moves to the right, assumes the smooth transition shape, and should leave a uniform flow behind it. However, in the first steps of integration, some numerical perturbations are generated around the shock. They will propagate on the two sides of the shock, along the characteristics ($u \pm a$). In fact, the perturbations on the low-pressure side are immediately swallowed by the moving shock, as well as the one traveling on the $u+a$ characteristic on the high-pressure side, while that running on $u-a$ behind the shock moves away from it. Depending on the shock intensity, this $u-a$ value can be positive (stronger shock) or negative (weaker shock) and the perturbation can then travel rightward or leftward, or, for the intermediate intensity of the shock, not propagate at all.

In Fig. 8, the paths of the shock (solid line) and of the $u-a$ characteristic (dashed line) on the high-pressure side, which originated at the initial location of the shock, are drawn for three intensities of the shock ($M_{sh}=1.5$, 2.0, 3.0). The symbols denote the location of the numerical perturbation, which looks like an undershoot in the almost uniform flow behind the shock. This consideration is useful in understanding some results shown in the following sections about the merging of shocks.

Expansion Shocks

These experiments are interesting in order to check the capability of a numerical procedure to avoid the unphysical capturing of an expansion shock. As initial conditions, let us assume a flow with a subsonic inlet and a supersonic outlet separated by a jump described by the Rankine-Hugoniot relationships, with the entropy decreasing across it. With reference to Fig. 9, this initial configuration is not stable and the jump evolves in time by generating the expansion fan (1-1), the contact surface (2), and a very weak shock (3), as can be predicted theoretically. It is interesting to note that, as already reported in Refs. 6 and 13 in connection with the scalar equation case and mentioned in Ref. 7 for Euler equations, the APP1 approach applied in its original form accepts this expansion shock as completely stable. This is due to the simulation of the expansion fan (1-1) with one vertical

line that separates regions a and c in Fig. 1. On the contrary, the APP2 and APP3 approaches generate the expansion fan, as shown in Figs. 3b and 4b, owing to the further splitting of wave 1 through the sonic point. The symbols refer to numerical results obtained by the second-order scheme with APP3 and show a good agreement even in describing the weak shock. A slight jump is still noticeable at the location of the initial expansion shock, but it is decreasing continuously in time.

Steady Flow in De Laval's Nozzles

These experiments refer to the prediction of transonic shockless flow in convergent-divergent ducts by a time-dependent technique. At the initial time, the nozzle is filled with a gas at rest, at the same levels of total temperature and pressure as a feeding reservoir. A diaphragm separates the end of the nozzle from an exit capacity where a suitable low pressure is prescribed. Suddenly, the diaphragm is removed and waves travel upstream in the duct. At the end of this physical transient, a steady-state configuration is achieved. The APP1, APP2, and APP3 approaches have been applied with the first-order scheme. From APP2 and APP3, completely stable steady numerical solutions are reached. The two sets of results are almost undistinguishable, but show some inaccuracy about the throat (sonic transition) by overestimating the pressure in the subsonic region and underestimating it in the supersonic one. With APP1, the results at the end of the physical transient are very much similar to those obtained with APP2 and APP3. For example, at $k=2000$, the three numerical solutions are almost identical. However, while those obtained with APP2 and APP3 are definitely stable in time, the solution from APP1 tends to shift slowly but continuously in time, building up an expansion shock at the throat. Figure 10 shows the exact levels of pressure (dashed lines) at the points $i=7$, 8 (respectively, ahead of and at the throat) and the numerical results that change in time from $k=1{,}000$ to 25,000, denoting the generation of an expansion shock. The numerical results obtained by the first- (triangles) and second- (circles) order schemes with APP3 are shown in Fig. 11, where the solid line refers to the exact pressure distribution. The small and completely stable jump can be seen about the sonic transition in the first-order solution, just as was found in Fig. 9 of Ref. 8.

These experiments refer to the nozzle geometry with an area variation given by $A=x/2+1/x$ and delimited between $x=1.08$ and 1.80.

Shock in a Divergent Nozzle

The divergent part the above nozzle geometry is now considered between $x=2.04$ and 3.0. The initial conditions are represented by a steady supersonic flow with prescribed the inlet Mach number ($M_{inl}=1.3037$). Suddenly the exit pressure (p_{ex}) is raised to a higher level corresponding to a steady flow with a shock located in the duct. A shock is then generated at the end and travels upstream until the steady configuration is reached. The exact pressure distribution along x is plotted as a solid line in Fig. 12 for different values of the exit pressure. The symbols refer to the results obtained by the second-order scheme with APP3.

Shock Tube

The results from the classical case of a shock tube are given in Fig. 13 in terms of density. The initial conditions are represented by a pressure ratio of 10 and a density ratio of 8. The numerical results at $t=1.75$ (second-order scheme with APP3) show a sharp description of the shock, good prediction of the expansion, but the contact surface is spread over about five intervals.

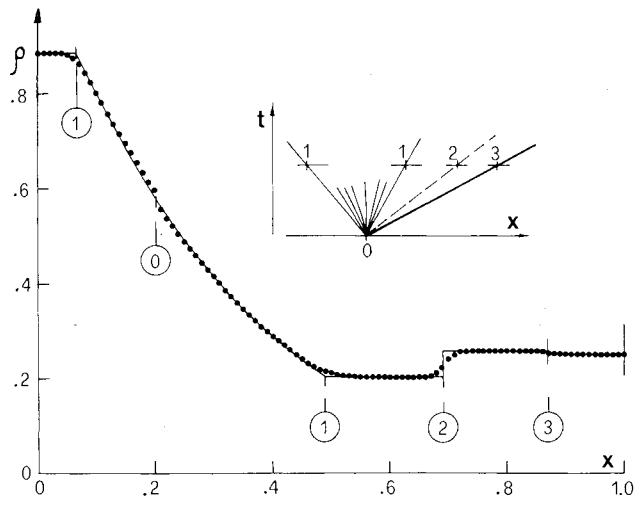

Fig. 9 Computed density distribution in the evolution of an expansion shock.

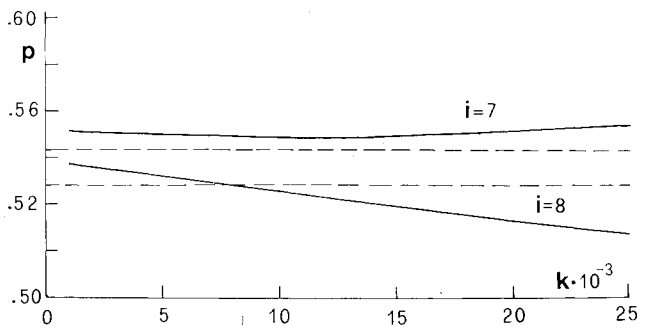

Fig. 10 Generation of an expansion shock at the throat of a convergent-divergent nozzle with approach APP1.

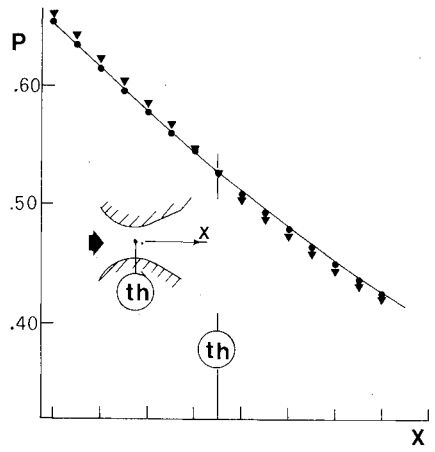

Fig. 11 Pressure distribution in a convergent-divergent nozzle computed with approach APP3.

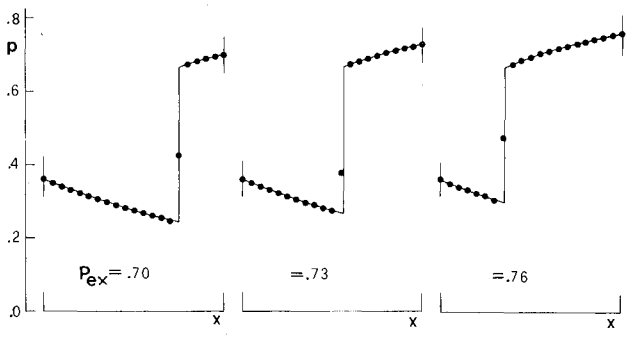

Fig. 12 Computed pressure distribution for a steady shock in a divergent nozzle.

Piston Problems

This example requires the use of a transformation of the independent variables. A piston moves suddenly rightward from rest to a constant velocity in a constant-area duct filled with gas at rest. The left boundary is represented by the piston and the right one is a closed end (piston with zero velocity). With b(t) and c(t) as the prescribed locations of the boundaries, the following transformation is used:

$$X=\frac{x-\mathrm{b}(t)}{\mathrm{c}(t)-\mathrm{b}(t)} \qquad T=t$$

The theoretical distribution of pressure along x is plotted in Fig. 14 at two different times. The symbols denote the numerical results (second-order and APP3).

Pulsating Flow

In order to check the accuracy of the second-order scheme, the following example of unsteady shockless flow is considered, where the exact solution can be predicted. In a constant-area duct, the total inlet pressure oscillates around a mean value and the Riemann invariant $[2a/(\gamma-1)-u]$ at the exit is kept constant.

It is very easy to predict exactly the flow properties at any point and at any time because of the "simple wave" nature of this flow. Numerical experiments have been worked out with different mesh sizes for the first- and second-order schemes with APP3, and the validity of the expected order of accuracy has been checked. The solid line in Fig. 15 denotes the exact behavior of the gas velocity during one cycle in the middle (x_m) and at the end (x_e) of the duct. The numerical results refer to the second-order scheme with APP3.

Interactions of Shocks

The last numerical experiments shown here regard the interaction of shocks (collision and merging). In the collision case, one shock is propagating rightward ($M_{s1}=2.0$) and the second leftward ($M_{s2}=1.5$), with the gas in between at rest. The interaction occurs at $t=0.0966$ and generates two transmitted shocks and a contact surface. The exact distribution of density along x is plotted as the solid line in Fig. 16 at three different time levels. The numerical results are obtained, here and in the following experiments, on the merging, by the second-order scheme with APP3. The description of the shocks is quite clear, except at the mean time ($t=0.138$) just after the interaction. At the largest time the shocks are still predicted very well, but some numerical perturbation that originated at the interaction is probably responsible for the less accurate prediction of the weak contact surface.

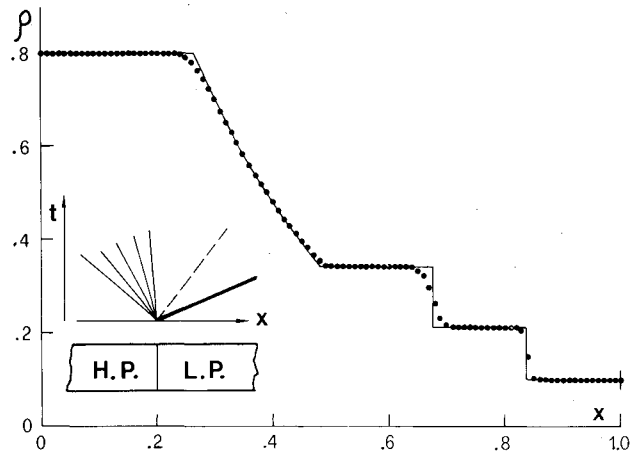

Fig. 13 Computed density distribution for a shock-tube problem.

The final example is about the merging of two shocks. Both travel rightward: the first propagates in a gas at rest and is the stronger ($M_{s1}=3.0$), while the second is going to overtake the first and is weaker ($M_{s2}=1.5$). The interaction occurs at $t=0.0504$ and generates the resultant strong shock, a contact surface, and an expansion fan. The exact distribution of pressure along x is plotted as a solid line in Fig. 17 at three time levels. The expansion fan is quite sharp. The numerical results are denoted by symbols. At $t=0.0434$, just before the interaction, the two shocks, still separated in the exact solution, are almost captured numerically in the resultant one. The flow behind it is far from uniform and seems to be affected by the numerical perturbations originated at the start of the computation where the initial data describe the two shocks with sharp transitions. This problem has been discussed previously in the example about the generation of the transition through shocks. At larger times, the shock is as usual predicted very well. On the contrary, the expansion fan, which is very narrow (over two intervals at the largest time) has been spread numerically over many intervals. Such a poor prediction can be ascribed both to the numerical perturbation seen in the previous example and to the lack of computational points for describing the expansion fan.

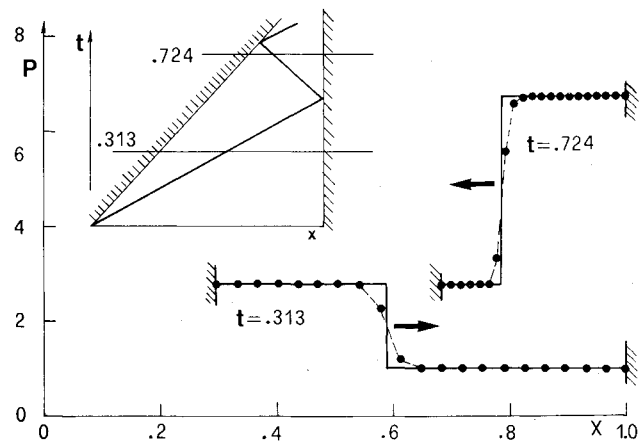

Fig. 14 Computed pressure distribution at two different times for the piston problem.

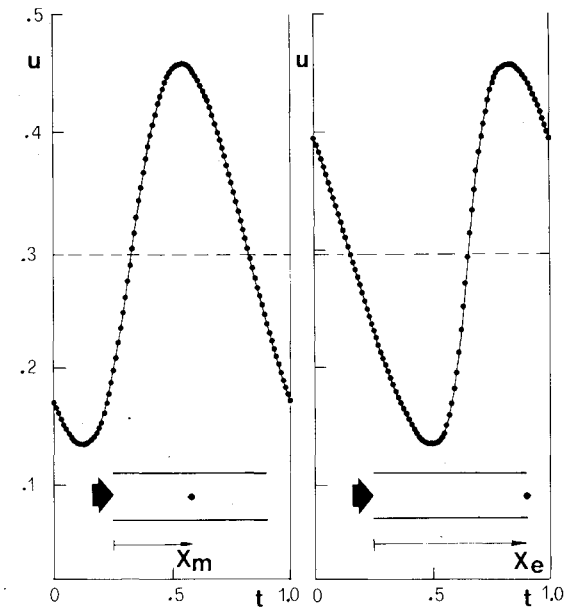

Fig. 15 Evolution in time of the velocity at two different locations along a duct with pulsating inlet flow conditions.

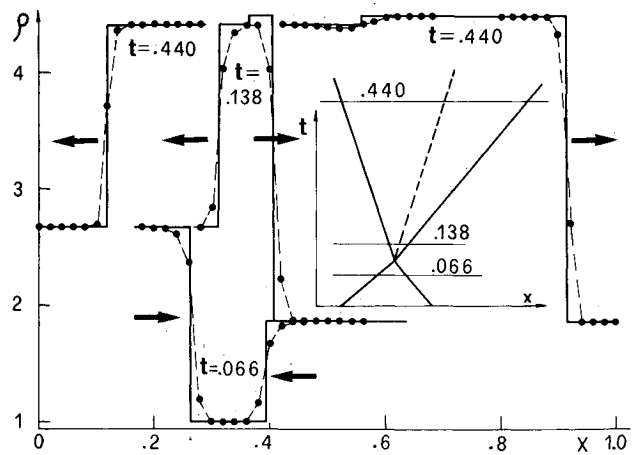

Fig. 16 Computed density distribution at three different times for the interaction of two opposite moving shocks.

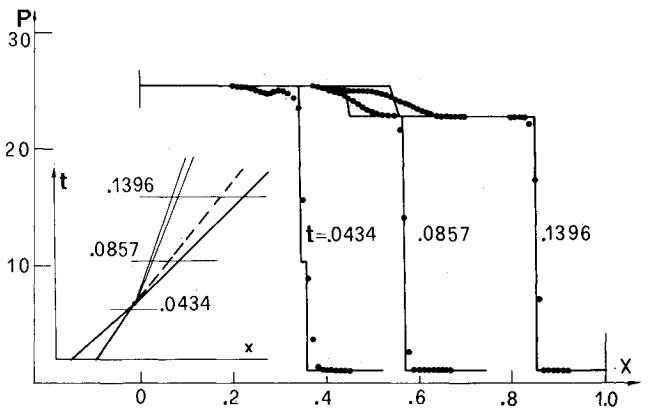

Fig. 17 Computed pressure distribution at three different times for the merging of two shocks.

Conclusions

Numerical methods based on the "flux-difference splitting" offer a very powerful tool for the prediction of unsteady compressible flows. They combine the feature of providing criteria in order to discriminate the correct information carried by propagating waves and the capability of correctly capturing shock waves. The approaches for operating the splitting of the difference in the flux considered in this paper (two presented recently and a third one proposed here) are based on approximate procedures for solving a Riemann problem.

They have been extended to the more general cases of variable-area ducts and of a transformation of the independent variables. A second-order upwind integration scheme has been considered in order to improve the accuracy. Procedures for predicting the flow at and near the boundaries were shown. Finally, a variety of numerical experiments have been presented and discussed.

The rather good quality of the numerical results corroborates the confidence in developing this kind of approach, even if it should be recognized that the work done for operating the splitting is, at least presently, extensive and time consuming. Also, the second-order scheme involves a large number of operations, a factor that must be considered. Moreover, some inaccuracies develop in nontrivial problems, such as in the interaction of shocks.

Acknowledgment

The author wishes to acknowledge support of this research by the Consiglio Nazionale delle Ricerche (Contributo No. 82.00087.07).

References

[1]Moretti, G., "The λ-Scheme," *Computers and Fluids*, Vol. 7, No. 3, 1979, pp. 191-205.

[2]Steger, J. L. and Warming, R. F., "Flux Vector Splitting of the Inviscid Gasdynamic Equations," *Journal of Computational Physics*, Vol. 40, 1981, pp. 263-293.

[3]Godunov, S. K., "A Finite-Difference Method for the Numerical Computation of Discontinuous Solutions of the Equations of Fluid Dynamics," *Matematicheskii Sbornik*, Vol. 47, 1959, pp. 271-290.

[4]Lombard, C. K., Oliger, J., and Yang, J. Y., "A Natural Conservative Flux Difference Splitting for the Hyperbolic Systems of Gasdynamics," *Lecture Notes in Physics*, Vol. 170, Springer Verlag, Berlin, New York, 1982, pp. 364-370.

[5]Roe, P. L., "The Use of the Riemann Problem in Finite Difference Scheme," *Lecture Notes in Physics*, Vol. 141, Springer Verlag, Berlin, New York, 1981, pp. 354-359.

[6]Osher, S. and Solomon, F., "Upwind Difference Schemes for Hyperbolic System of Conservation Laws," *Mathematics of Computation*, Vol. 38, 1982, pp. 339-377.

[7]Roe, P. L., "Approximate Riemann Solvers, Parameter Vectors and Difference Schemes," *Journal of Computational Physics*, Vol. 43, 1981, pp. 357-372.

[8]Chakravarthy, S. and Osher, S., "Numerical Experiments with the Osher Upwind Scheme for the Euler Equations," AIAA Paper 82-0975, 1982.

[9]Pandolfi, M., "A Contribution to the Numerical Prediction of Unsteady Flows," AIAA Paper 83-0121, 1983.

[10]De Neef, T. and Moretti, G., "A Shock Fitting for Everybody," *Computers and Fluids*, Vol. 8, 1980, pp. 327-334.

[11]Van Leer, B., "Towards the Ultimate Conservative Difference Scheme, IV: A New Approach to Numerical Convection," *Journal of Computational Physics*, Vol. 23, 1977, pp. 276-299.

[12]Zannetti, L. and Moretti, G., "Numerical Experiments on the Leading Edge Flow Field," *5th AIAA Computational Fluid Dynamics Conference Proceedings*, AIAA, New York, 1981, pp. 149-155.

[13]Van Leer, B., "On the Relation between the Upwind-Differencing Schemes of Godunov, Engquist-Osher and Roe," ICASE Rept. 81-11, March 1981.